

Design and fabrication of compact Ge-on-SOI coupling structure

Jianfeng GAO, Junqiang SUN (✉), Heng ZHOU, Jialin JIANG, Yang ZHOU

Wuhan National Laboratory for Optoelectronics, School of Optical and Electronic Information,
Huazhong University of Science and Technology, Wuhan 430074, China

© Higher Education Press and Springer-Verlag GmbH Germany, part of Springer Nature 2018

Abstract In this paper, we have proposed and demonstrated a simple approach to fabricate vertical integrated structure for coupling between active germanium (Ge) waveguide and silicon-on-insulator (SOI) waveguide. The active Ge waveguide is sputtered after etching the underlying passive silicon (Si) waveguide. This method scuttles away from the difficulty involved in the waveguide fabrication by avoiding the etching process for the Ge waveguide, and thereby the waveguide quality is improved. The influences of the coupling structural parameters on the coupling loss are analyzed and discussed. The optimizing parameters are obtained for the fabrication. The minimal coupling loss is experimentally measured about 2.37 dB, and variation tendency of coupling loss against the structural parameters is consistent with the theoretical result. The proposed approach offers an effective path for vertical coupling between Ge and SOI optical components.

Keywords taper coupler, integrated optics device, guided waves, silicon-on-insulator (SOI) waveguide, germanium (Ge) waveguide, active Ge device, Ge-on-SOI coupling structure

1 Introduction

Active germanium (Ge) devices [1–3] in silicon-based (Si-based) integrated optoelectronic chips have been recognized as the future development direction of the photonic chip because the potential direct bandgap of Ge lies within the communication C band. This integrated chip is inseparable from the coupling between the active waveguide and the passive waveguide. The vertical coupler between two layers is a key component which remains to

be researched. A double-grating scheme has been proposed to provide coupling between two vertically stacked silicon-on-insulator (SOI) waveguides [4]. But the coupling efficiency is only 29% as this scheme utilizes radiation modes which have high transmission losses. Another parallel approach is the microring that couples light from the upper waveguide into the SOI slab [5]. The function of microring vertical coupler is limited since strip or ridge waveguide is more preferred by integration applications. Taper couplers have drawn much attention as they are simple in construction and flexible for use in integrations [6–8]. We proposed a design of compact and efficient polarization-insensitive taper coupler for SiGe photonic integration in our previous work [9]. The taper length is greatly decreased by utilizing the mode interference effect.

The passive waveguide is generally SOI waveguide with width of 750 nm and height of 220 nm, to ensure the characteristics of single-mode transmission [10]. Active devices are typically grown upon passive waveguides, and both ends of active devices are laterally tapered waveguides to guarantee that the optical field is coupled between active and passive waveguides. But the etching technology for Ge material is currently not mature enough. The sidewall roughness of the waveguide after etching is large, resulting in the deterioration of the optical transmission performance of the waveguide.

In this paper, a vertical integrated structure is proposed to couple optical fields between active Ge waveguide and Si waveguide. This coupling structure contains different segments with different widths and inclination angles. The impacts of waveguide width and height and inclination angle on the coupling efficiency are numerically calculated and analyzed. The optimal structural parameters for the coupling structure are obtained. A novel approach is demonstrated to fabricate the supposed tapered coupler. To overcome the difficulty involved in the Ge etching and improve sidewall roughness, the Ge is directly sputtered into the mold formed in the photoresist. The fabrication

process is described in detail. The coupling loss is experimentally measured and is about 2.37 dB. The results indicate that the variation trend of coupling loss against the structural parameters coincides with the theoretical results. The proposed method provides an alternative to fabricate vertical coupling structure for integrated SOI optical devices. The fabricated Ge-on-SOI structures provide a feasible solution for integrated Ge modulators [11,12] and photodetectors [13,14]. Several steps of doping and metal depositions are required to form a lateral p-i-n structure. As the taper length is only 3 μm , the coupling structure is benefit to the applications of large scale optical circuit integrations.

2 Mode analysis

The proposed laterally tapered coupler with active Ge waveguide are shown in Fig. 1(a). Two different routes of light transmission can occur within this structure, as shown in Fig. 1(b). When the light propagating in the SOI waveguide encounters the tapered coupler, a large part of optical power will be coupled into the active waveguide through the Route I. The light coupling along the Route I is corresponding to the fundamental mode coupling. For this laterally tapered coupling structure, the changes of width, thickness and sidewall inclination of the active tapered waveguide will directly affect the coupling efficiency. The remaining optical fields in Route II will oscillate between the active waveguide and the SOI waveguide layer. The structural parameters of active waveguide are discussed as follows to analyze their impacts on the transmission efficiency of the fundamental mode. For the SOI based photonic integration, the transverse electric (TE) mode in

the SOI waveguide is generally preferred to achieve small bending radius and low loss. Therefore, only the TE mode is calculated for the design. The mode distributions are calculated by the finite-difference time-domain (FDTD) MODE Solutions using the Palik dielectric constants of Si and Ge [15]. The refractive indexes of Si and Ge are 3.477 and 4.257 respectively at the wavelength of 1550 nm.

Figure 2 shows the variation of the fundamental mode scattering against the width of the active Ge waveguide. With the increase of the width of the tapered active waveguide, the fundamental mode scattering first increases and then decreases, and there is a significant scattering peak at the specific taper width. The width of the active tapered waveguide corresponding to the scattering peak is defined as the resonant width of the coupling structure [9,16,17]. As can be seen from Fig. 2, the scattering amount of the fundamental mode increases sharply near the resonance width, so the taper angle of the tapered active waveguide near the resonant width is generally designed to be small to avoid large scattering loss of fundamental mode.

When the height of the active waveguide is increased from 200 to 400 nm, the value of the scattering peak of the fundamental mode is significantly increased and the resonant width is slightly reduced. This indicates that the height of the active waveguide has a great influence on the fundamental mode scattering, but has little effect on the resonant width. For practical application, the heights of the passive waveguide and the upper waveguide are both predetermined. Because the upper waveguide contains the integrated active device. We choose the Ge waveguide height of 200 nm, as the 200 nm Ge film has attracted much attention recently [18,19].

As a supplement, the influence of the sidewall inclina-

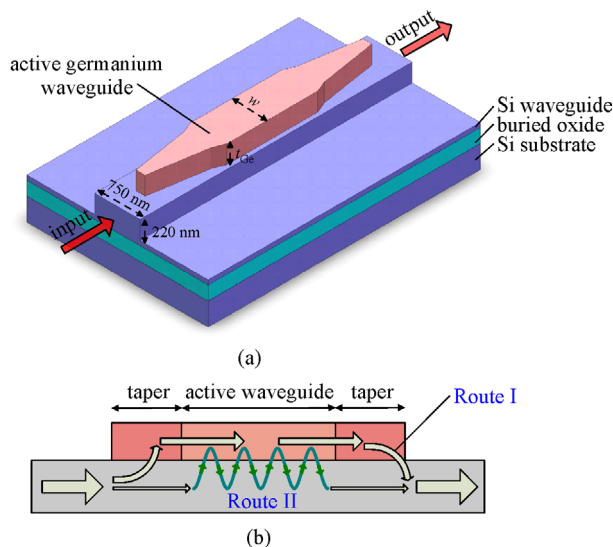


Fig. 1 (a) Schematic diagram of the Ge active waveguide and laterally tapered coupler; (b) two routes of optical transmission within the coupling structure

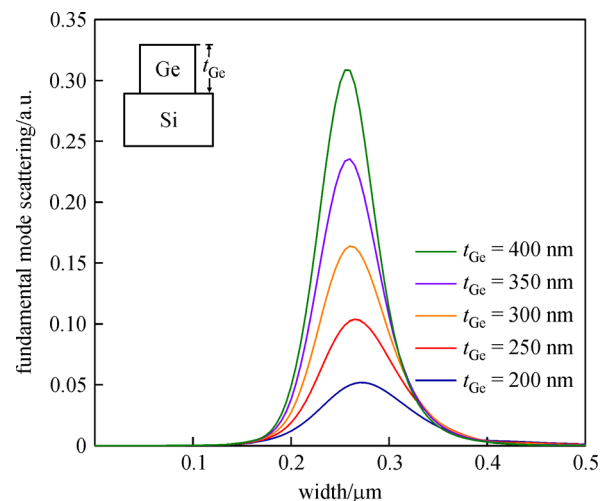


Fig. 2 Fundamental mode scattering as a function of the active waveguide width in the coupling structure under different active waveguide heights t_{Ge} , with the sidewall inclination of 90°

tion α of the active waveguide on the scattering of the fundamental mode is also discussed. Figure 3 illustrates the simulated fundamental mode scattering as a function of sidewall inclinations. With the increase of the sidewall inclination of the active waveguide, the value of the scattering peak of the fundamental mode increases, and the resonant width corresponding to the peak point also increases. Compared with the height of the active waveguide, the change of the sidewall inclination of the sidewall has a larger influence on the resonant width. The increase of the sidewall inclination will bring in a large scattering loss of fundamental mode. Since both the larger waveguide width and larger sidewall inclination of the active waveguide are readily to achieve. It is necessary to compromise the scattering loss and the waveguide width to determine the appropriate sidewall inclination in the actual fabrication.

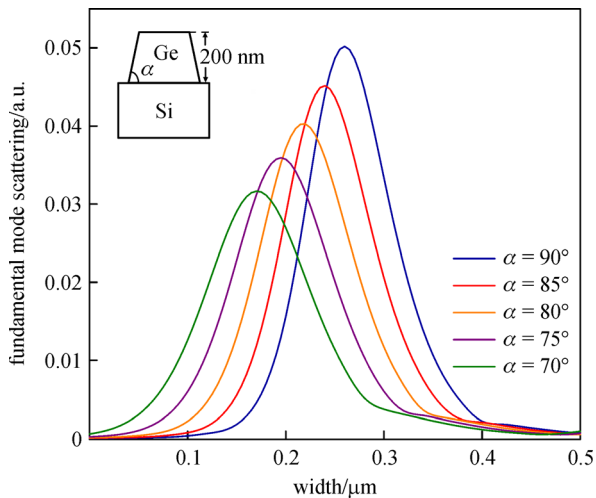


Fig. 3 Fundamental mode scattering as a function of the active waveguide width in the coupling structure under different sidewall inclinations of the active waveguide, with the active waveguide height of 200 nm

3 Taper design

To optimize the shape of the taper-shaped active waveguide, the taper will be segmented. According to the fundamental mode scattering curves, the taper-shaped active waveguide can be divided into three sections, as shown in Fig. 4. The design principle is that the resonant width lies within the width range of middle section. The taper angle of the middle section should be smaller to produce a smooth and strong fundamental mode coupling. Compared with the middle section, the strength of fundamental mode scattering is much lower in the tip and tail section, so the taper angle can be larger to shorten the device length. Considering that the waveguide with width less than 100 nm is difficult to achieve in the fabrication process, the tip section is eliminated. Thus the

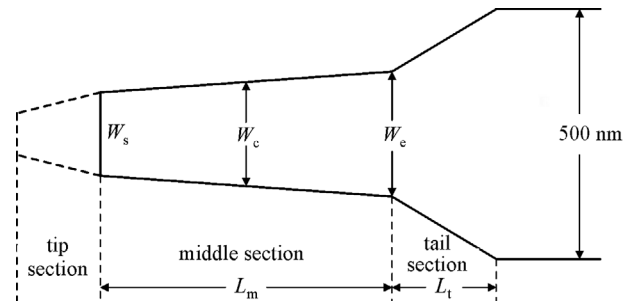


Fig. 4 Schematic diagram of the designed tapered active waveguide. W_s and W_e are the starting width and ending width of the middle section

designed taper only has two sections, with the middle and tail section. The length parameters are set as $L_m = 2.5 \mu\text{m}$ and $L_t = 0.5 \mu\text{m}$ to achieve a compact design.

To achieve a compact and efficient coupling structure, the taper shape should be designed appropriately. The taper behavior is dominated by the central width W_c and the width difference $W_e - W_s$. The central width is defined as the average of the starting width and the ending width in the middle tapered section. Figure 5 shows the variations of coupling efficiency as a function of central width under different sidewall inclinations when the width difference of the middle section is kept unchangeable. It can be seen from Fig. 5 that when the central width is around 260 nm, the maximum coupling efficiency is obtained. When the central width of the middle section deviates from 260 nm, the coupling efficiency decreases greatly. Hence the central width of the middle section is set at 260 nm. It is interesting that the degeneration of coupling efficiency at smaller W_c tends to be moderate when the sidewall inclination exists. Figure 6 displays variations of the coupling efficiency against the width difference $W_e - W_s$ with the central width of 260 nm. As can be seen from Fig. 6, with the increase of

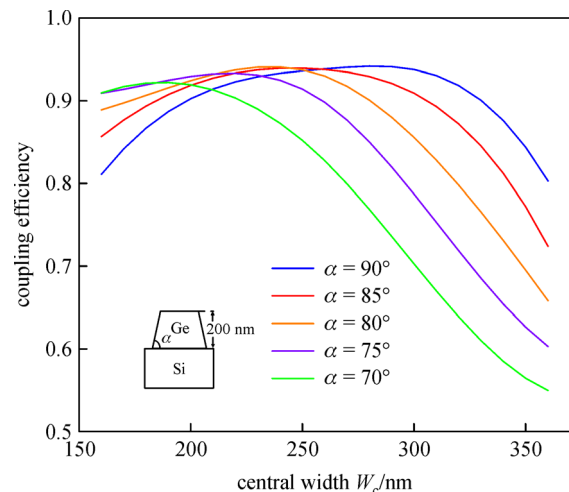


Fig. 5 Coupling efficiency as a function of central width of the middle section in the taper when the width difference $W_e - W_s$ is kept at 200 nm

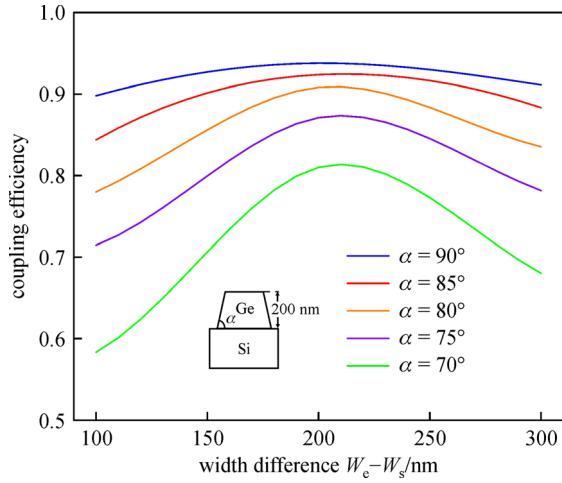


Fig. 6 Coupling efficiency as a function of width difference of the middle section in the taper with the central width of 260 nm

the width difference, the coupling efficiencies change gradually. The maximum coupling efficiencies occur when the width difference is around 200 nm. With the width difference of 200 nm and central width of 260 nm, a strong resonant coupling transfers the light power into the upper waveguide and a proper taper angle ensures an efficient conversion of optical field to the Ge waveguide mode. When the width difference is larger than 200 nm, the upwards power transfer is not sufficient. At the region of width difference smaller than 200 nm, the coupling efficiency is mainly limited by the large taper angle of the tail section.

4 Transmission simulation

To inspect the performance of the designed tapered coupler, FDTD algorithm is utilized to simulate the transmission of optical fields for different shapes of tapered couplers. Figure 7 illustrates the optical field

transmission image in the coupling structure when the central width W_c of the middle section is less than, equal to, and greater than the resonant width of 260 nm. It can be found from Fig. 7 that when the central width deviates from 260 nm significantly, the optical power in the passive waveguide cannot be completely transferred to the active waveguide, but oscillates between the two waveguides through the Route II. Since a considerable portion of the fundamental mode scattering peak falls at the tail section with a large taper angle, a large amount of the power in the fundamental mode is coupled into the first-order mode. This will cause mode interference between fundamental and first-order mode, leading to the power oscillation transmission between the active waveguide and the passive waveguide. Figure 8 shows the optical field distribution in the tapered coupler under different values of width difference $W_e - W_s$. It can be found that the optical power oscillates obviously with the decrease of the width difference. This behavior can be ascribed to mode interference and is similar to the phenomenon taking place in the front position of the varied central width.

In two-section tapered coupling structure, the middle section as the main region of the coupling, should be designed a smaller taper angle and wider width range corresponding to the scattering peak to suppress the scattering loss of the fundamental mode. On the contrary, the taper angle of the tail section should be appropriately increased to shorten the device length.

5 Fabrication and discussion

5.1 Fabrication of coupling structures

Ge-on-SOI coupling structure can be used widely in large scale integrated circuits [20]. A layer of Ge material is epitaxially grown on the SOI substrate, and a set of different sizes of active devices and passive waveguides can be fabricated through etching process. However, the current etching technology for Ge material is not mature

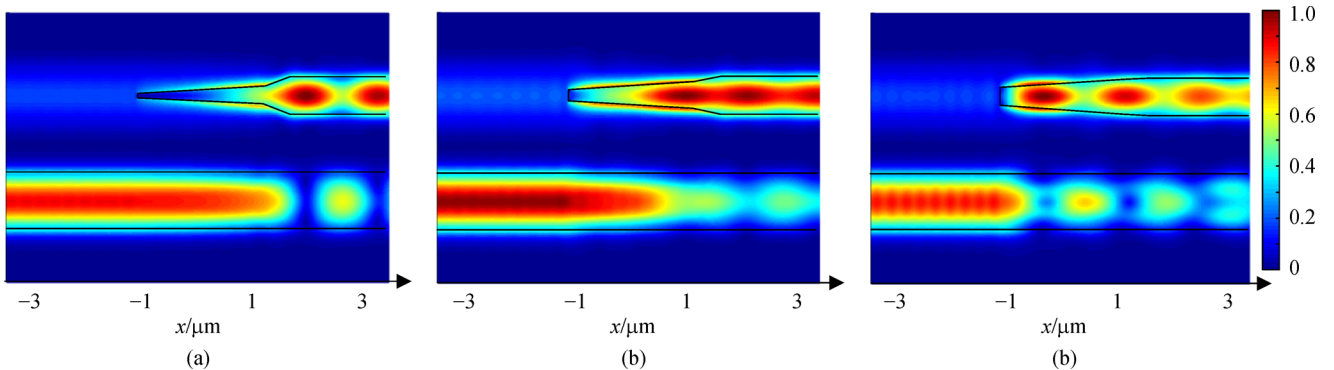


Fig. 7 For different central widths W_c , the normalized profile of the electric field distribution at the middle of Ge and SOI layers. (a) $W_c = 160$ nm; (b) $W_c = 260$ nm; (c) $W_c = 360$ nm. The width range $W_e - W_s = 200$ nm

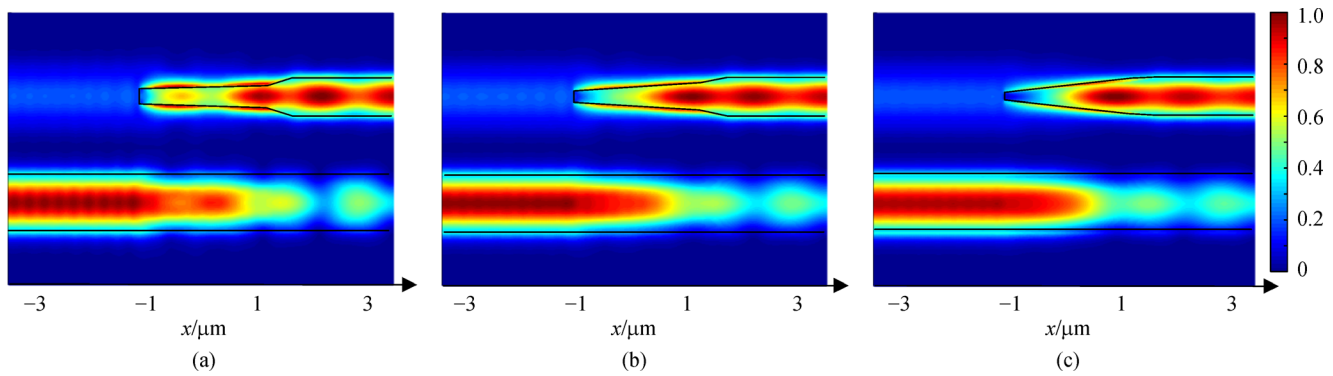


Fig. 8 For different width differences $W_e - W_s$, the normalized profile of the electric field distribution at the middle of Ge and SOI layers. (a) $W_e - W_s = 100$ nm; (b) $W_e - W_s = 200$ nm; (c) $W_e - W_s = 300$ nm. The central width $W_c = 260$ nm

enough. Etching the Ge waveguide will not only result in a large sidewall roughness, but also cause the inclination in the waveguide sidewall, and hence has the difficulty in keeping the steepness of the sidewall. Additionally, the etching depth is usually slightly larger than the thickness of the Ge material layer. Consequently, the surface smoothness of the underlying Si layer is spoiled, causing the increase of transmission loss of the passive waveguide beneath the active Ge waveguide. Taking into account the above shortcomings in etching the Ge waveguide, we scuttle away from the etching process in the fabrication of Ge waveguide. Instead, a mold for the coupling structure is first formed in the photoresist and then the Ge material is sputtered into the mold. With this method, the perfect surface of the Si waveguide will not be damaged. The mature inductively coupled plasma (ICP) etching is only employed to fabricate the Si waveguide [21,22], the vertical and mirror-like sidewall of the passive Si waveguide can be conveniently obtained. The complete fabrication process for Ge-on-SOI coupling structure is given in detail as follows (see Fig. 9).

Since the Ge-on-SOI coupling structure requires two steps of electron beam lithography to fabricate waveguide structure in different material layers, it is necessary to deposit a metal mark on the SOI substrate to ensure alignment accuracy between the two waveguides. Figure 9 (a) shows that metal mark is created on the SOI substrate to align the passive Si waveguide to the active Ge waveguide. Here, the electron beam evaporation is utilized to deposit a layer of 20 nm nickel and 100 nm gold on the SOI substrate. The SOI substrate needs to be cleaned after the metal marking has been made.

Figure 9(b) illustrates that the photoresist is spun and coated on the SOI substrate. The photoresist for making the pattern of the passive Si waveguide is ZEP520A [23], which has the advantages of high resolution and good steepness of sidewall. After finishing coating the photoresist, the wafer should be baked to harden the ZEP520A film.

The size of the Ge-on-SOI coupling structure is relatively small, and the width of the passive waveguide

is in the order of 100 nm. To ensure the fabrication accuracy, the electron beam lithography is used to form the pattern of the passive waveguide. Figure 9(c) displays that the waveguide pattern is shaped on the photoresist after the electron beam lithography. After the exposure is completed, the substrate requires photographic developing and fixing in xylene and acetone solution.

Figure 9(d) shows that the passive Si waveguide is made through the ICP etching process. The preferred waveguide sidewall roughness and steepness are ensured by selecting the appropriate etching rate and etching selection ratio.

Figure 9(e) manifests the passive Si waveguide after removing the photoresist on the substrate surface. To eliminate the photoresist much more thoroughly, the substrate is ultrasonically cleaned. After removing the photoresist, the atomic force microscopy and scanning electron microscopy are used to check the shape of the passive waveguide. The transmission loss of the passive Si waveguide is measured to select some qualified substrates that can be then used to fabricate active tapered waveguide.

Figure 9(f) illustrates that the photoresist is spun and coated again on the substrate with the passive waveguide. Taking into consideration that the Ge material will be sputtered in the next step, we choose polymethylmethacrylate (PMMA) [24] as the photoresist here. PMMA is suitable for evaporation stripping process, because it not only has a high resolution, but also is flexible to remove.

Figure 9(g) shows that the shape of the coupling structure with the active waveguide is formed in the PMMA photoresist after electron beam lithography. The exposure, photographic developing and fixing processes are similar to those used for the passive waveguides. Since the PMMA is a positive photoresist, the photoresist at the exposure position is detached after photographic developing and fixing, and thus the shape of the coupling structure is shown up.

After the mold of the coupling structure including the active waveguide is developed, the Ge material is sputtered to fill in the mold with the corresponding shape. Figure 9(h) shows that the Ge material is filled into the shape mold by sputtering. During fabrication, the general etching is not

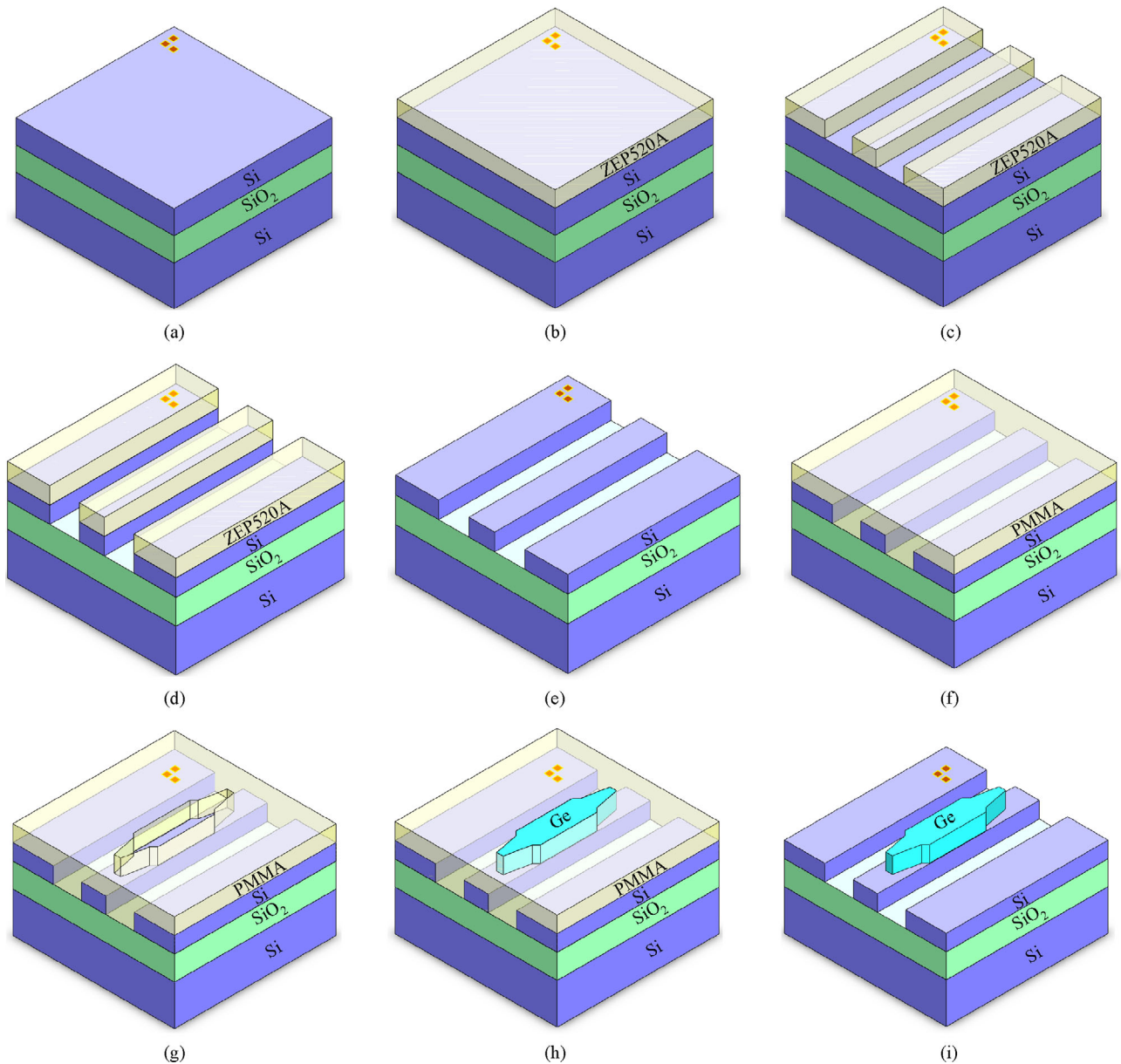


Fig. 9 Schematic diagram of the fabrication process of Ge-on-SOI coupling structure. (a) Making metal mark; (b) coating ZEP520A; (c) electron beam lithography; (d) ICP etching; (e) removing the photoresist ZEP520A; (f) coating PMMA; (g) electron beam lithography; (h) sputtering Ge material; (i) removing the photoresist PMMA

adopted to realize the tapered Ge waveguide. To improve the adhesion of Ge material to the passive Si waveguide, it is necessary to reduce the sputtering rate of Ge material and increase the contact area between the Ge and the Si material. In addition, selecting the appropriate sputtering conditions can avoid shedding of the Ge material during removing of the PMMA photoresist.

Figure 9(i) illustrates the coupling structure with the active waveguide after cleaning the PMMA photoresist. Since the tapered Ge waveguide has a small tip size of about 100 nm, ultrasonic cleaning is prohibited to prevent the tip of the tapered waveguide from breaking.

After carrying out the above process step by step, the

fabrication of Ge-on-SOI coupling structure is completed. Figure 10 is a scanning electron microscope (SEM) image of Ge-SOI coupling structure. It is found from Fig. 10 that the tapered structure has two sections with different taper angles.

5.2 Experimental measurement of the fabricated coupling structure

To measure the coupling efficiency of the Ge-on-SOI coupling structure, we set up an experimental platform for optical coupling alignment. Cone lensed optical fibers and photonic crystal gratings are utilized to achieve the optical

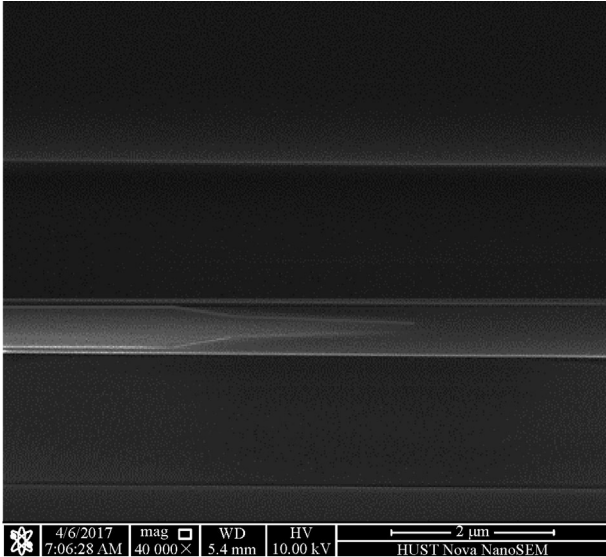


Fig. 10 SEM image of the fabricated Ge-on-SOI coupling structure

coupling between the optical fiber and the fabricated coupling structure. The schematic diagram of the coupling alignment between optical fibers and photonic crystal gratings is shown in Fig. 11. The input and output fibers are connected with the laser and the optical power meter respectively to measure the coupling efficiency. The passive waveguide in the coupling structure is aligned to the photonic crystal grating at both ends to realize the optical coupling between the optical fiber and the waveguide. At beginning, the angle of the lensed fiber related to the grating coupler is adjusted at the proper angle for reaching the lowest coupling loss. The smallest coupling loss is measured about 25 dB at the coupling angle of approximately 10° . Then two lensed fibers are moved to the vicinity of the surface of the photonic crystal gratings. Finally, the coupling angle and lensed fiber position are fine-tuned through three dimensional precision adjustment frame so that the maximum power can be obtained in the optical power meter.

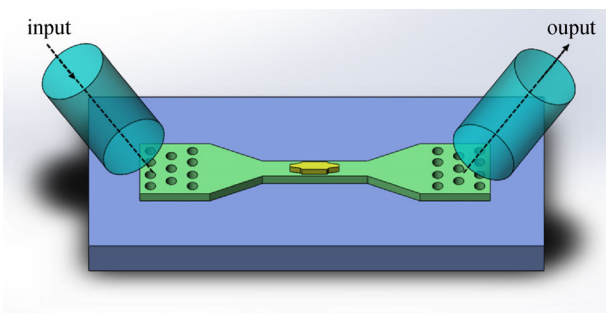


Fig. 11 Schematic diagram of the coupling alignment between optical fibers and photonic crystal gratings

There are several reasons causing the transmission loss for the Ge-on-SOI coupling structure. The main optical losses are the coupling loss between the active waveguide and the passive waveguide, the absorption loss of Ge material and the waveguide scattering loss. The absorption loss can be ascribed to the larger absorption coefficient of Ge material at the wavelength of 1550 nm. The waveguide scattering loss arises from the sidewall roughness. The absorption loss can be obtained by the material absorption coefficient, optical propagation length and optical field distributions. The scattering loss can be acquired through the simulation of the coupling structure at the given waveguide sidewall roughness and the sidewall inclination angles. The absorption and scattering loss are calculated for several coupling structures with different shapes, and the data are given in Table 1. During the calculation, the FDTD algorithm is used to simulate the optical field distributions.

We fabricated several tapered coupling structures with different taper shapes and parameters to verify their coupling efficiencies. The measured average loss of coupling structures with different shapes and parameters are listed in Table 2. Through the coupling alignment platform, the total optical power loss of the Ge-on-SOI coupling structure is measured. The coupling loss is estimated by subtracting the absorption and scattering loss. It can be seen from Table 1 that the absorption and scattering loss are the main factors leading to the increase of the total optical power loss for the three groups. Moreover, the Ge material has a strong energy absorption for the laser with the wavelength of 1550 nm, resulting in the large absorption loss. Besides, ultrasonic cleaning is not applied to protect the tapered structure from being damaged during the fabrication. A residue of little part of photoresist on the Ge waveguide surface cannot be cleaned completely, giving rise to the increase of optical loss. In addition, an alignment error is inevitably introduced during the fabrication between the active waveguide and the passive waveguide, causing the increase of the coupling loss. For the three different shapes of the tapered coupling structures, there is no significant difference for the total measured optical power loss. However, when the width range of the middle section is 160–360 nm, the coupling loss of the coupling structure is lower than that of the other two structures. This implies that variation tendency of coupling loss with the structural parameters is in accordance with the simulation result.

6 Conclusions

A vertical integrated structure for coupling between the active Ge waveguide and the passive SOI waveguide is proposed and investigated theoretically and experimentally. The impacts of the active waveguide width and height on the fundamental mode scattering of the coupling

Table 1 Absorption loss and the scattering loss for different taper shapes

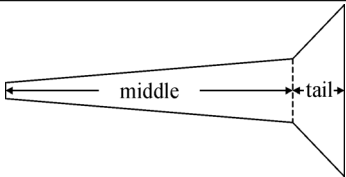
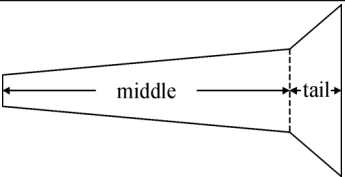
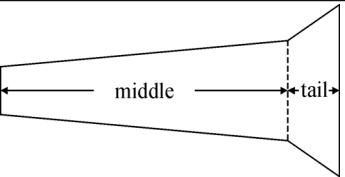
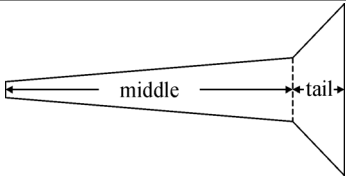
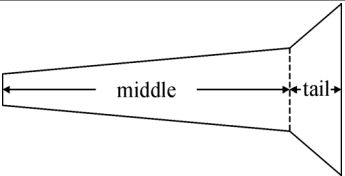
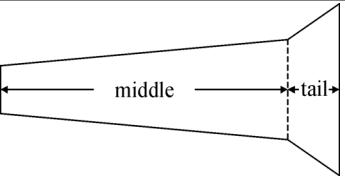
parameters			
width range of the middle section	60–260 nm	160–360 nm	260–460 nm
absorption loss	4.62 dB	4.70 dB	4.65 dB
scattering loss	3.18 dB	3.10 dB	3.02 dB

Table 2 Coupling loss and the total loss for the different taper shapes

parameters			
width range of the middle section	60–260 nm	160–360 nm	260–460 nm
coupling loss	2.49 dB	2.37 dB	2.67 dB
total loss	10.29 dB	10.17 dB	10.34 dB

structure are analyzed. According to the fundamental mode scattering and the current manufacturing level, a tapered coupling structure with two sections is designed and the detailed structural parameters are explained and discussed. The middle section plays a crucial role in waveguide coupling, and hence its width difference corresponding to the scattering peak is chosen to improve the coupling efficiency. Since the active devices in the Si-based integrated optoelectronic chip are mostly Ge or SiGe materials, the etching process of these materials is still not mature enough. The deterioration of the sidewall steepness and roughness of the active device pose an obstacle to achieve integrated optical components with high performance. To avoid this deficiency, the designed Ge-on-SOI coupling structure is fabricated by sputtering the Ge material into the mold formed in advance on the upper layer after etching the underlying passive Si waveguide. Several coupling structures with different taper shapes and parameters are fabricated and verified. It is found that both the material absorption loss and sidewall scattering loss are the main factors causing the increase of the total optical power loss. The measurement results indicate that the influences of the structural parameters on the coupling loss are in good agreement with the theoretical simulated results. Our scheme provides an effective way to fabricate coupling structure for Si-based integrated optical devices.

Acknowledgements This work was supported by the National Natural Science Foundation of China (NSFC) (Grant No. 61435004).

References

- Liu J, Sun X, Camacho-Aguilera R, Kimerling L C, Michel J. Ge-on-Si laser operating at room temperature. *Optics Letters*, 2010, 35 (5): 679–681
- Ren S, Rong Y, Claussen S A, Schaevitz R K, Kamins T I, Harris J S, Miller D A B. Ge/SiGe quantum well waveguide modulator monolithically integrated with SOI waveguides. *IEEE Photonics Technology Letters*, 2012, 24(6): 461–463
- Liu J, Pan D, Jongthammanurak S, Wada K, Kimerling L C, Michel J. Design of monolithically integrated GeSi electro-absorption modulators and photodetectors on a SOI platform. *Optics Express*, 2007, 15(2): 623–628
- Dong P, Kirk A G. Compact double-grating coupler between vertically stacked silicon-on-insulator waveguides. *Applied Optics*, 2005, 44(35): 7540–7547
- Lu Z. Efficient fiber-to-waveguide coupling through the vertical leakage from a microring. *Optics Letters*, 2007, 32(19): 2861–2863
- Vusirikala V, Saini S S, Bartolo R E, Agarwala S, Whaley R D, Johnson F G, Stone D R, Dagenais M. 1.55- μm InGaAsP-InP laser arrays with integrated-mode expanders fabricated using a single epitaxial growth. *IEEE Journal of Quantum Electronics*, 1997, 3(6): 1332–1343
- Lamponi M, Keyvaninia S, Jany C, Poingt F, Lelarge F, de Valicourt G, Roelkens G, Van Thourhout D, Messaoudene S, Fedeli J M, Duan G H. Low-threshold heterogeneously integrated InP/SOI laser with a double adiabatic taper coupler. *IEEE Photonics Technology Letters*, 2012, 24(1): 76–78
- Bauters J F, Davenport M L, Heck M J R, Doylend J K, Chen A,

- Fang A W, Bowers J E. Silicon on ultra-low-loss waveguide photonic integration platform. *Optics Express*, 2013, 21(1): 544–555
9. Zhou H, Sun J, Gao J, Jiang J, Zhou Y. Design of compact and efficient polarization-insensitive taper coupler for SiGe photonic integration. *Optics Express*, 2016, 24(21): 23784–23797
 10. Kwon M S, Shin J S, Shin S Y, Lee W G. Characterizations of realized metal-insulator-silicon-insulator-metal waveguides and nanochannel fabrication via insulator removal. *Optics Express*, 2012, 20(20): 21875–21887
 11. Liu J, Beals M, Pomerene A, Bernardis S, Sun R, Cheng J, Kimerling L C, Michel J. Waveguide-integrated, ultra-low energy GeSi electro-absorption modulators. *Nature Photonics*, 2008, 2(7): 433–437
 12. Gao J, Sun J, Jiang J, Zhou H, Zhou Y. Design and analysis of electro-absorption modulators with uniaxially stressed Ge/SiGe multiple quantum wells. *Optics Express*, 2017, 25(10): 10874–10884
 13. Feng D, Liao S, Dong P, Feng N, Liang H, Zheng D, Kung C, Fong J, Shafiqi R, Cunningham J, Krishnamoorthy A V, Asghari M. High-speed Ge photodetector monolithically integrated with large cross-section silicon-on-insulator waveguide. *Applied Physics Letters*, 2009, 95(26): 261105
 14. Fidaner O, Okyay A K, Roth J E, Schaevitz R K, Kuo Y H, Saraswat K C, Harris J S, Miller D A B. Ge-SiGe quantum-well waveguide photodetectors on silicon for the near-infrared. *IEEE Photonics Technology Letters*, 2007, 19(20): 1631–1633
 15. Palik E D. *Handbook of Optical Constants of Solids*. New York: Academic Press, 1985
 16. Lee C W, Chin M K, Iyer M K, Popov A. Asymmetric waveguides vertical couplers for polarization-independent coupling and polarization modes splitting. *Journal of Lightwave Technology*, 2005, 23(4): 1818–1827
 17. Lee C W. A review of polarization dependence applications for asymmetric waveguides vertical couplers in compound semiconductor indium phosphide. *International Journal of Optics*, 2011, 2011: 164023
 18. Gassenq A, Guilloy K, Osvaldo Dias G, Pauc N, Rouchon D, Hartmann J M, Widiez J, Tardif S, Rieutord F, Escalante J, Duchemin I, Niquet Y M, Geiger R, Zabel T, Sigg H, Faist J, Chelnokov A, Reboud V, Calvo V. 1.9% bi-axial tensile strain in thick germanium suspended membranes fabricated in optical germanium-on-insulator substrates for laser applications. *Applied Physics Letters*, 2015, 107(19): 191904
 19. Sukhdeo D S, Nam D, Kang J H, Brongersma M L, Saraswat K C. Direct bandgap germanium-on-silicon inferred from 5.7% $\langle 100 \rangle$ uniaxial tensile strain. *Photonics Research*, 2014, 2(3): A8–A13
 20. Fedeli J M, Cioccio L D, Marris-Morini D, Vivien L, Orobtcouk R, Rojo-Romeo P, Seassal C, Mandorio F. Development of silicon photonics devices using microelectronic tools for the integration on top of a CMOS wafer. *Advances in Optical Technologies* 2008, 2008: 412518
 21. Liu H C, Lin Y H, Hsu W. Sidewall roughness control in advanced silicon etch process. *Microsystem Technologies*, 2003, 10(1): 29–34
 22. Sökmen Ü, Stranz A, Fündling S, Merzsch S, Neumann R, Wehmann H H, Peiner E, Waag A. shallow and deep dry etching

of silicon using ICP cryogenic reactive ion etching process. *Microsystem Technologies*, 2010, 16(5): 863–870

23. Okada T, Fujimori J, Aida M, Fujimura M, Yoshizawa T, Katsumura M, Iida T. Enhanced resolution and groove-width simulation in cold development of ZEP520A. *Journal of Vacuum Science & Technology B Microelectronics and Nanometer Structures*, 2011, 29(2): 021604
24. Pudiš D, Šušlik L, Kubicová I, Škriniarová J, Martinček I. Advanced optical methods for patterning of photonic structures in photoresist, III–V semiconductors and PMMA. In: *Proceedings of 17th Slovak-Czech-Polish Optical Conference on Wave and Quantum Aspects of Contemporary Optics*. 2010, 774608



Jianfeng Gao received the B.E. degree in optical information science and technology from Huazhong University of Science and Technology, Wuhan, China, in 2014. He is currently pursuing the Ph.D. degree in optical engineering with Wuhan National Laboratory for Optoelectronics, Huazhong University of Science and Technology.

His research interests include integrated germanium waveguides, germanium devices and Ge/SiGe multiple quantum wells electro-absorption modulators.

As a Student Member of the Optical Society of Hubei Province, he has helped to organize the invited lectures of Wuhan Optoelectronics Forum.



Junqiang Sun received the Ph.D. degree in electronic physics and optoelectronics from Huazhong University of Science and Technology, Wuhan, China, in 1994. From September 2000 to September 2001, he was a research associate at Hong Kong University of Science and Technology. From June 2005 to December 2005, he was a research fellow at the School of Information Technology and Engineering, University of Ottawa, Canada. He is currently a professor at the Wuhan National Laboratory for Optoelectronics and the vice Director for the functional laboratory of Optoelectronic Devices and Integration.

As a project leader, he carried out the research projects of the National Natural Science Foundation of China, National “863” high technology programs, Program for New Century Excellent Talents in University by the Ministry of Education of China, Outstanding Youth Foundation of Hubei Province, Major Technologies R&D Program of Wuhan City and Technology of Huawei of China. He has published more than 100 papers in refereed journals and conference proceedings. He has achieved 11 patents for invention, and won four provincial and ministerial awards.

His current research interests include integrated optical devices, all-optical signal processing based on nonlinear optical waveguides, microwave photonic devices and technologies, novel fiber lasers and optical amplifications, optical fiber sensing technologies based on optical nonlinearities.



Heng Zhou received the B.E. degree in optical information science and technology from Harbin Institute of Technology, Harbin, and the M.S. degree from Huazhong University of Science and Technology, Wuhan, China, in 2014 and 2017, respectively.

She is currently a Product Development Engineer with Huawei Hisilicon department, Shenzhen, China. Her current research interests include integrated optoelectronic devices and image recognition. She has helped to organize the 2015 Annual Meeting of OSA/SPIE.



Jialin Jiang received his B.E. degree from Huazhong University of Science and Technology, Wuhan, China, in 2014. Now he is a Ph.D. candidate at Wuhan National Laboratory for Optoelectronics, Huazhong University of Science and Technology, Wuhan, China.

His current research interests include silicon-based light sources, modulators and other integrated optoelectronics devices with applications in communications and signal processing.



Yang Zhou received the B.E. degree in physics from Huazhong Normal University, Wuhan, China, and the M.S. degree from Huazhong University of Science and Technology, Wuhan, China, in 2013 and 2017, respectively.

He is currently a Product Development Engineer with ZTE photonics, Nanjing, China. His current research interests include integrated Ge modulators, photo detectors and passive Ge devices.